AIAA JOURNAL
Vol. 46, No. 5, May 2008

Unsteady Aperiodic Behavior of a Periodically Disturbed Tip-Leakage Vortex

Ruolong Ma* and William J. Devenport†
Virginia Polytechnic Institute and State University, Blacksburg, Virginia 24061-0203

DOI: 10.2514/1.13539

A tip-leakage vortex periodically disturbed by upstream vortical inflow is studied in a cascade facility. The object of this paper is an improved understanding of the time-resolved scale and form of the coherent structures of the tip-leakage flow, especially the aperiodic motion of the coherent turbulence structure within the tip-leakage vortex, which dominates the turbulence kinetic energy. This information is relevant to the understanding and prediction of broadband tip-leakage noise by the rotor blades and intermittent cavitation in propulsion pumps. The cascade facility has a moving endwall on which vortex-generator pairs are attached upstream of the blade row to generate an unsteady periodic vortical inflow representative of an array of stator necklace vortices. The downstream tip-leakage vortex is disturbed periodically by the vortical inflow shed by those vortex generators. Phase-averaged two-point correlations are measured near the trailing edge of the cascade. The measurement results clearly show that organized, intense, large-scale aperiodic motion exists at each phase time within the tip-leakage-vortex region. The aperiodic fluctuations obtained by linear stochastic estimation have a magnitude of less than $\pm 0.15U_\infty$ in all three velocity directions and appear to be organized large-scale structures. The streamwise fluctuations appear as coexisting "rush" and "retard" regions with different shapes, and the crossflow fluctuations appear to be clockwise/anticlockwise or doubletlike rotating vortical structures with different strengths and center positions. These aperiodic fluctuations make the estimated instantaneous velocity field significantly different from the phase-averaged periodic velocity field.

Introduction

THIS paper follows the study by Ma and Devenport [1,2] on the unsteady behavior of tip-leakage flow downstream of a compressor rotor, the tip-leakage vortices being disturbed periodically by the wakes shed by upstream inlet guide vanes. Tip-leakage vortices are known to be associated with noise generation in aircraft engines and intermittent cavitation in the flow immediately downstream of the blade tip in propulsion pumps. However, the literature contains few references to studies of the effects of stator–rotor interaction on tip-leakage vortices, and no detailed time-resolved data are available to disclose the mechanism or consequences of the unsteady interaction [1].

To reproduce this phenomenon in an idealized environment free of confounding influences, a linear cascade and moving-wall model are used. The wind tunnel, schematically shown in Fig. 1, features a moving endwall to simulate the relative motion between the rotor and casing, with vortex-generator pairs attached to the moving endwall to produce the vortical inflow. The generator pairs create an array of counter-rotating vortex pairs that simulate, in an idealized way, the periodic flow shed from the casing junctions of a row of inlet guide vanes. The junction wakes are dominated by necklace, corner separation, and other secondary flow vortices and are thus reasonably represented by vortex-generator wakes.

In the first two papers of this study by Ma and Devenport [1,2] (hereafter referred to as MD), phase-averaged hot-wire measurements of the inflow vortices and downstream tip-leakage-vortex flow are presented as functions of streamwise position, presence of inflow disturbance, and tip gap. Here, phase indicates the relative position between the cascade blade and vortex-generator pair. These measurements reveal that the inflow vortices shed by the vortex-generator pair, which are very weak (one or two orders weaker than that of the tip-leakage vortex), can produce significant phase-averaged fluctuations in the size, strength, structure, and position of the tip-leakage vortex (see MD [1]). Tip-gap size has a nonlinear influence on these effects. For small tip gaps, the fluctuations appears to be a consequence of simple superposition between inflow vortices and the tip-leakage vortex, suggesting that direct interaction is the dominant mechanism. However, the fluctuations increase significantly in magnitude with the increase of tip gap and are primarily a consequence of the inflow vortices interfering with the shedding of circulation from the blade tip (see MD [2]). The measurement data give, for the first time, detailed information on the periodic unsteady motion of the tip-leakage vortex in the presence of periodic inflow disturbances.

To further reveal and understand the behavior of tip-leakage vortices, the aperiodic behavior should be investigated because most of such motion is aperiodic. To examine this, the contributions of the periodic and aperiodic fluctuations to the total turbulence kinetic energy (TKE) are presented in Fig. 2 based on the data from MD [1]. The TKE contribution of periodic fluctuations (Fig. 2b) is calculated as

$$k_{\text{periodic}} = \tfrac{1}{2}\overline{(\langle u_i\rangle_p - \bar{u}_i)(\langle u_i\rangle_p - \bar{u}_i)}$$

where u_i denotes the velocity component; the overbar denotes the time-averaged value; and the symbol $\langle\,\rangle_p$ denotes the phase-averaged value at phase p, which represents the 256 instantaneous position of the vortex-generator pairs relative to the blades. The TKE contribution of aperiodic fluctuations (Fig. 2c) is approximately obtained by subtracting the periodic contribution from the total TKE:

$$k = \tfrac{1}{2}\overline{(u_i - \bar{u}_i)(u_i - \bar{u}_i)}$$

These data are taken some 30% of the blade spacing axially downstream the trailing-edge plane of the center passage between blades 4 and 5. These pictures show the flow as it would appear from upstream. The two vertical wakes shed by blades 4 and 5 are shown, respectively, on the right and left edges of the figure, and visible at the bottom of these figures is the tip-leakage vortex shed from blade 4

Received 20 September 2004; revision received 20 August 2006; accepted for publication 3 January 2008.

*Graduate Assistant, Department of Aerospace and Ocean Engineering; currently Hessert Lab, University of Notre Dame. Senior Member AIAA.

†Professor, Department of Aerospace and Ocean Engineering, 215 Randolph Hall. Associate Fellow AIAA.

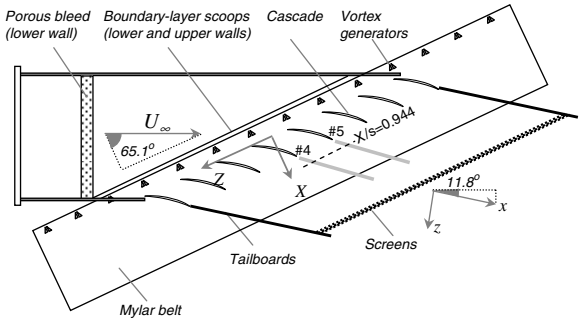

Fig. 1 Plan view of the cascade wind-tunnel test section at Virginia Polytechnic Institute and State University (not to scale).

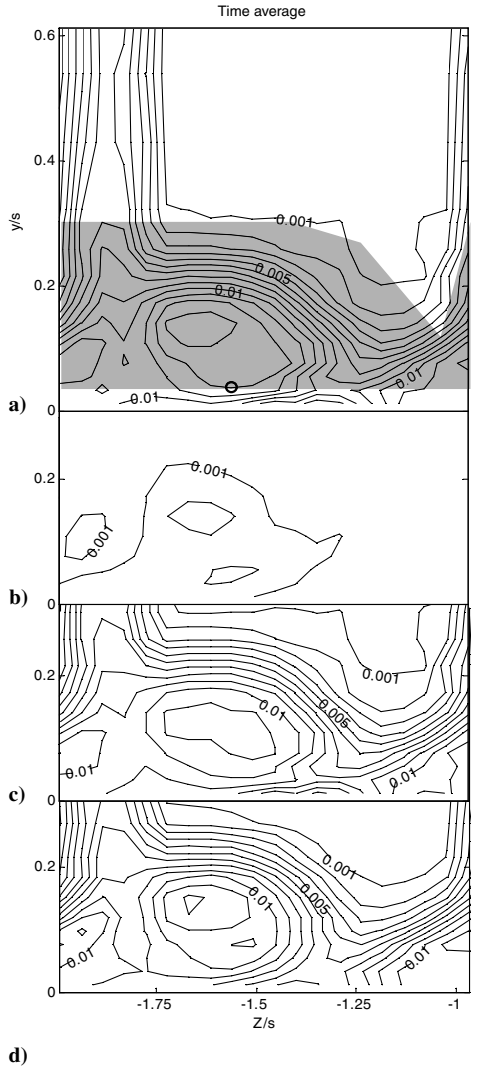

Fig. 2 Time-averaged TKE and the contributions from periodic and aperiodic fluctuations for a 3.3%c tip gap at $X/s = 0.944$: a) total TKE k/U_∞^2, b) TKE due to periodic fluctuations, c) TKE due to aperiodic fluctuations, and d) TKE of no-vortex-generator case. Contours in steps of 0.001 from 0 to 0.014. The gray region in the top plot shows the extent of the two-point measurement grid associated with the fixed-probe location ($y_f/s = 0.038, Z_f/s = -1.56$) indicated by a circle at the bottom edge of the gray region.

and the associated boundary-layer flow. The direction of the endwall motion is from right to left.

Figure 2b shows that the contribution from the periodic flow is quite small (about 10% of the total TKE within the vortex core), and the contribution from the aperiodic flow is the strongly dominant portion, which consists of two parts: the aperiodic flow associated with the inflow disturbance and the aperiodic flow not associated with the inflow disturbance. The difference between these two parts can be further examined by comparing Fig. 2c with Fig. 2d, the TKE distribution measured without introduction of the inflow disturbances (no vortex generators on the moving wall, and only the relative motion between rotor blades and casing is modeled). In the vortex core region, the maximum TKE level in Fig. 2c is hardly lower than that of Fig. 2d, but has a larger region suggesting that aperiodic fluctuations are at the same level as those of the no-inflow-disturbances case, they are just somewhat smeared by periodic motions. The introduction of the inflow disturbances does not produce or reduce the aperiodic fluctuations.

The objective of the present paper is thus to improve the understanding of the physical structure of the tip-leakage flow, especially the aperiodic structure, through the phase-averaged two-point correlation data of this flow, to provide benchmark data for the calibration and testing of prediction methods. In this paper, the results of phase-averaged two-point velocity correlation measurements made for tip gap at 3.3% chord are presented. This information provides insight into the time-resolved scale and form of the coherent structures within the tip-leakage flow, especially the aperiodic part of those structures. This is apparent through the following explanation.

The instantaneous flow associated with generators can be decomposed into a mean flow U_g, a periodic fluctuation u'_{g-p}, and an aperiodic fluctuation u'_{g-ap}:

$$u_g = U_g + u'_{g-p} + u'_{g-ap}$$

where the subscript g denotes the contribution associated with the inflow disturbances. Then the disturbed tip-leakage flow would be

$$u = U + U_g + u'_{g-p} + u'_{g-ap} + u'_t$$

where U denotes the mean flow not associated with inflow disturbances, and u'_t denotes the true turbulence fluctuation not associated with the inflow. It is obvious that the time-averaged mean value only includes U and U_g, but the phase-averaged mean value contains an additional term, the periodic component of the fluctuation u'_{g-p}, and the variance of phase-averaged mean only consists of the aperiodic and true turbulence fluctuations. Thus, phase-averaged two-point correlation measurement results will reveal the time-resolving scale and form of the aperiodic part of the coherent structures within the tip-leakage flow and will tell us how the aperiodic structures are modified by the inflow disturbances.

Given phase-averaged two-point correlation data, the instantaneous velocity flowfield can be estimated through linear stochastic estimation (Adrian [3]). The results are suitable for comparison with an LES solution and are also important for understanding the physics of the turbulence structures. Furthermore, two-point space–time cross-correlation tensor or wave-number frequency spectra are required to predict the broadband turbulence interaction noise (Devenport et al. [4], Devenport and Glegg [5], and Wenger et al. [6]) when the leakage vortex flow impinges on downstream elements. The phase-averaged two-point correlation information is thus critical for both understanding and predicting the generation of phase-locked broadband tip-leakage noise by the rotor blades.

Wenger et al. [6] presented and analyzed two-point correlation data of tip-leakage flow measured in the same facility used in the present study, but without wall motion and inflow disturbances. The flow in this condition is an idealized model of the flow downstream of a rotor row in a compressor or aircraft-engine fan. The authors found that the tip-leakage vortex is not subject to low-frequency wandering motions and has large highly anisotropic structure within it: a very elongated elliptical region of strong correlation that extends diagonally across the vortex. The Wenger et al. work has provided improved understanding of the coherent structures within tip-leakage vortex as well as insight into its potential to produce the broadband noise seen in the stator frame.

The present paper complements the study of MD [1,2] by providing a detailed address of the aperiodic behavior of the

tip-leakage vortex. It is also a further extension of the Wenger et al. [6] work toward prediction of broadband rotor–stator interaction noise. Phase-averaged two-point data are obtained for the first time for periodically disturbed tip-leakage flow. The flow phenomenon and the involved mechanism are further revealed and understood. More details of this study are described by Ma [7].

Two-Point Measurements and Data Reduction

Measurements are made in the same cascade facility using the same hot-wire instrumentation and procedures as those described by MD [1]. The blades of the tunnel are chosen as the third stage of GE core compressor rotor-B blades, and the blade shape and cascade configuration of this wind tunnel are found to be able to represent the flow in propulsion pump rotors, compressor rotors, and aircraft engine fans (see Muthanna and Devenport [8]). The eight blades are mounted with an adjustable tip gap above a plane moving endwall. The cascade geometry data are given in Table 1. The nominal inlet freestream velocity U_∞ is 24.5 ± 0.5 m/s, corresponding to a chord Reynolds number at 27°C of $398,000 \pm 8100$.

The lower endwall is covered by a 0.25-mm-thick Mylar belt propelled at a speed equal to the pitchwise component of the freestream. Half-delta-wing vortex-generator pairs (described in detail by MD [1]) are glued to the belt with their trailing edges $0.29\ \text{s} \pm 0.02\ \text{s}$ (the uncertainty in location reflects the limits of the axial drift of the belt) upstream of the blade row. The spacing between generator pairs is set to be equal to the blade spacing so that a periodic phase-averaged flow can be generated on the rotor frame. On the running belt, the vortex generators only experience the axial component of the freestream; the counter-rotating vortices shed by the generator pairs is thus traversing along the axial direction on the belt. The leading vortex is larger, with a height of $7\%c$ at 0.135 s upstream of the cascade leading edge (see MD [1] for details). The circulation is about $0.003U_\infty s$, which is about two orders of magnitude smaller than the typical circulation in the tip-leakage vortices. An optical system is used to sense the instantaneous generator location and to construct a phasing signal by subdividing each time interval into 256 equal periods representing the instantaneous position of the vortex-generator pairs relative to the blades. At phase 0, generator pairs are axially upstream of the center point of each blade passage entrance. At phase 128, generator pairs are axially upstream of the blade leading edges. An increment in the phase number of 1 represents an increment in time of 41 μs and a tangential motion of the generators of $s/256$ (i.e., almost 1 mm).

Cascade-aligned coordinates (X, y, Z) are used to define measurement positions, and downstream flow-aligned coordinates (x, y, z) are used to define the flow velocity components, illustrated in Fig. 1. The origin of the cascade coordinates is on the lower endwall midway between the leading edges of the two center blades (numbers 4 and 5). The downstream flow-aligned coordinates are rotated about the y axis, compared with the cascade coordinates, the angle between X and x being 53.3 deg.

Phase-averaged two-point measurements are made for a single tip gap of $3.3\%c$ by using two of the same miniature four-sensor three-component hot-wire probes with a measurement volume of 0.5 mm^3. The computer-controlled traverse system allows the moving probe be moved in both the y and Z directions and allows the fixed probe to be moved in only the Z direction, with a resolution of 0.025 mm. The measurement location is downstream of the center passage between blades 4 and 5 at $X/s = 0.944$, the same location as the single-point measurements presented by MD [1]. One probe (the fixed probe) is set at a fixed location ($y_f/s = 0.038$, $Z_f/s = -1.56$), indicated in Fig. 2a, which is just a little below the tip-leakage-vortex core so that correlations inside the tip-leakage vortex would be revealed. As long as the fixed probe is set within the tip-leakage-vortex region, the pattern of the two-point correlation measurement results should be insensitive to the fixed-probe location. A second probe (the moving probe) is then positioned at some 220 points around the fixed probe using the two-axis traverse gear. Each point corresponds to a different pitchwise separation ΔZ between the probes and a different spanwise separation Δy. The gray region in Fig. 2a shows the extent of the measurement grid. Points are taken at a greater density for smaller separations than for large separations, in anticipation of the shape of the correlation function. The minimum probe separation is 5.1 mm and the minimum change in probe separation between probes is 2.5 mm. At each point pair, 100 records (each 16,384 points in length) are recorded from each of the eight hot-wire sensors at a rate of 25.6 kHz.

Table 1 Cascade geometry data

Blade chord c, mm	254
Cascade spacing s, mm	236
Blade span, mm	254
Stagger angle, deg	56.9
Inlet angle, deg	65.1
Turning angle, deg	11.8

Because of the limitations of the traverse system, measurements are made over the left and right sides of the measurement grid separately. For both sets of measurements, the moving probe is initially positioned in the potential core to obtain the correct rotation angles. After the moving-probe alignment is known, the rotation angles of the fixed probe are determined by comparing the data taken at the fixed-probe position, respectively, using the moving and fixed probes. The rotation angles are also adjusted to minimize the overall mismatch of the velocity and stress component distributions between the left and right sides of the grid. The data sets, with different alignment of the probes relative to the flow, can thus be rotated into the downstream freestream-aligned coordinates (x, y, z).

The two-point phase-averaged correlation coefficient is defined as

$$R_{ij}(y_f, Z_f, y, Z, \tau_p) = \frac{\langle u_i'(y_f, Z_f, \tau_p) u_j'(y, Z, \tau_p)\rangle_p}{\sqrt{\langle u_i'^2(y_f, Z_f, \tau_p)\rangle_p}\sqrt{\langle u_j'^2(y_f, Z_f, \tau_p)\rangle_p}}$$

where (y, Z) denotes the moving-probe position. Note that no summation is applied. The first subscript index i denotes the direction of measured flow velocity at the fixed-probe position. The second subscript index j denotes the direction of measured flow velocity at the moving-probe position. Only zero-time-delay two-point correlation is considered here. The time-averaged single-point and two-point statistics are calculated from the phase-averaged statistics. The uncertainties of the measured two-point second-order correlations are calculated for 20:1 odds using the method of Kline and McClintock [9], and the results are 3% for a quantity of $\delta(R_{uu}, R_{vv}, R_{ww})$.

Results and Discussion

In this section, both the moving- and fixed-probe data are first examined by comparing them with the single-point data presented by MD [1], which is necessary for judging the two-point correlation data. Then time- and phase-averaged two-point correlation data are presented, discussed, and compared with the Wenger et al. [6] time-averaged two-point data. Finally, linear stochastic estimation is applied to educe probable features of the instantaneous velocity field of the flow. All of the data are plotted in the same format as the single-point data presented by MD [1]. The two-point correlations are plotted with respect to the moving-probe position, with the fixed-probe position indicated in the plots. For phase-averaged and phase-locked data, the Z location of the vortex generators at a specific phase time is also indicated by a triangle pair.

Data Validation

The comparison of the time-averaged moving-probe data (not presented here, see Figs. 5.4a and 5.4d in Ma [7]) and the time-averaged single-point data (see Figs. 7b and 8b in MD [1]) displays very good agreement except for a few small differences. One difference is that the width of the wake of the moving-probe data appears to be smaller than that in the single-point data, because the measurement grid is very sparse in the wake region for the two-point

measurements. Also, the streamwise velocity component of the moving-probe data is a little lower in the tip-leakage-vortex-core region than that of the single-point data. We think this is due to the presence of the fixed probe during the two-point measurements. The contours of streamwise vorticity (not shown here) also exhibit a pattern similar to that of the single-point data (Fig. 10b in MD [1]). The only difference is that the strong vorticity level of the leakage flow underneath the blade tip does not appear to be due to the sparse measurement grid there, and the contour level near the fixed-probe point seems a little higher, due to the dense grid there and the possible effect of probe interference.

The time-averaged fixed-probe data (shown in Figs. 5.6a and 5.6d in Ma [7]) are then compared with the moving-probe data (Figs. 5.4a and 5.4d in Ma [7]), measured at the same fixed point, and found to be consistent with the moving-probe data. They are fairly uniform as plotted with respect to the moving-probe position. However, little nonuniformity exists, especially between the left and right sides, which is because of the day-to-day drift and the error in repositioning the hot-wire probe. This nonuniformity is minimized by rotating the fixed-probe data of each side and making the data consistent with the average of the moving-probe data measured at the fixed-probe position of both left and right sides. On each side, there is also negligible nonuniformity, mainly due to the moving-probe interference during the measurements.

In brief, the moving- and fixed-probe data are consistent with the single-point data presented in MD [1]. This confirms the accuracy of the two-point correlation data.

Two-Point Correlations

The time-averaged second-order two-point correlation coefficients $R_{ij}(y_f, Z_f, y, Z)$ are presented in Fig. 3. The contours of all nine components of R_{ij} are plotted with respect to the moving-probe position (y, Z) in a step of 0.1 from -1 to 1. Both the fixed-probe position and time-averaged center position of the tip-leakage vortex are indicated. The vortex center position is calculated from the path of the phase-averaged center, successfully tracked using the maximum phase-averaged streamwise velocity deficit.

Significant time-averaged correlations are found existing in the flow, especially in the tip-leakage-vortex region; their magnitude and scale reveal the tip-leakage flow structures. The scale of the positive or negative regions is on the same order of (or even larger than, in most two-point correlation components) the scale of the tip-leakage vortex. This suggests the presence of large-scale turbulence structure or, more likely, large-scale motion of the tip-leakage-vortex flow.

Consider, for example, the R_{uu} component to examine the magnitude and extent of these correlation coefficients in Fig. 3. Not surprisingly, it is large and positive compared with the fixed probe. The peak correlation in this region is 0.65, the difference from one being due to the minimum separation of the two probes. This positive region is located underneath the time-averaged vortex center. It extends 0.15 s to either side, 0.06 s just above the fixed probe and 0.15 s above the fixed probe to the right side, like a thumb. However, there is a large negative region that forms an arc centered on the thumb, which surrounds the positive region. The lowest negative correlation region is -0.42 and is found 0.12 s above and 0.1 s to the left of the positive peak. The time-averaged vortex center is between the minimum and the positive peak and close to the former. Most parts of the arc are just outside the tip-leakage-vortex region indicated by the streamwise velocity deficit, which means that the u fluctuation outside the tip-leakage vortex is opposite of that in the tip-leakage vortex. This R_{uu} pattern is consistent with a clockwise rotating structure with opposite streamwise velocity fluctuations existing within it. The positive region is due to the secondary leakage flow near the wall, and the negative region is due to the rest of the secondary rotating motion of the tip-leakage vortex. There are two other positive correlation regions that appear just to be the wake.

For other correlation components, we can see in R_{vv} that there is a positive region next to the fixed probe in which the peak is 0.66. It extends to 0.05 s to either side and 0.25 s above the fixed probe. The time-averaged vortex center is around the middle of this positive region. There is a symmetric negative region, with a lower magnitude than that of the positive region, next to the positive region; this also suggests a vortical structure. In R_{ww}, there is a large positive region next to the fixed probe with the peak equal to 0.74. The positive region extends 0.2 s to both sides and 0.15 s above the fixed probe. The time-averaged vortex center is located at the top of this positive region. Outside the positive region, there is a big negative region that almost covers the whole of the rest of the measurement section but with very small magnitude. For the remaining components, there are no peaks at the fixed point. But significant correlation and organized pattern still exist in the measurement section, especially in the tip-leakage-vortex region.

As mentioned before, time-averaged R_{ij} includes both periodic and aperiodic fluctuations, whereas phase-averaged $\langle R_{ij} \rangle$ only includes the aperiodic fluctuations. The difference between them is

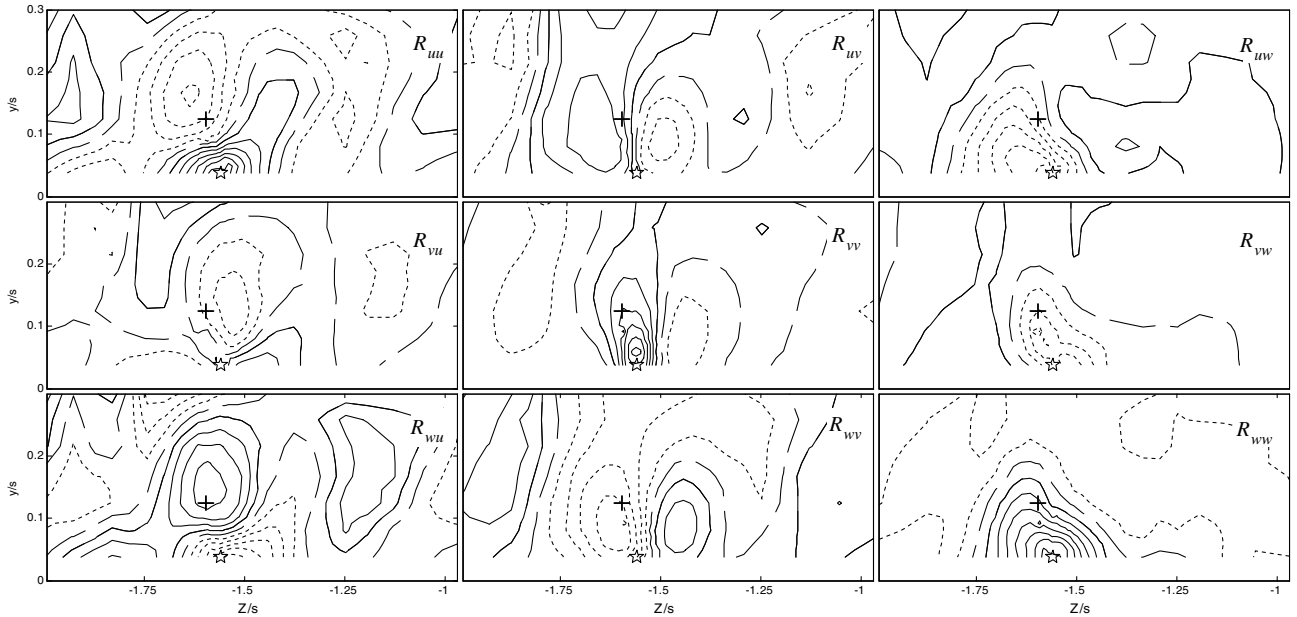

Fig. 3 Time-averaged zero-time-delay two-point correlation coefficients for 3.3%c tip gap at $X/s = 0.944$, plotted as a function of moving-probe position. Fixed probe is at $(y_f/s = 0.038, Z_f/s = -1.56)$. Contours are in steps of 0.1 from -1 to 1, dotted-negative levels, dashed-zero, solid-positive levels. The pentagram denotes the fixed-probe position and the plus sign denotes the time-averaged vortex center.

the contribution of periodic fluctuations. To see the formation and scale of both kinds of fluctuations, the phase-averaged $\langle R_{uu} \rangle$ at eight equal-interval phases (0, 32, 64, 96, 128, 160, 192, and 224) are plotted in Fig. 4a, and the time- averaged R_{uu} less the phase-averaged $\langle R_{uu} \rangle$ at the same eight phases are plotted in Fig. 4b. The fixed-probe position and the phase-averaged vortex center position tracked by MD [1] are also indicated. Figure 4b approximately represents the periodic contribution, because some cross terms contributed from both periodic and aperiodic motions are still included.

Quite different flow patterns are shown in Fig. 4. For $\langle R_{uu} \rangle$, the same kind of vortex feature as shown in the time-averaged R_{uu} is found. The correlation magnitude is very high within the tip-leakage-

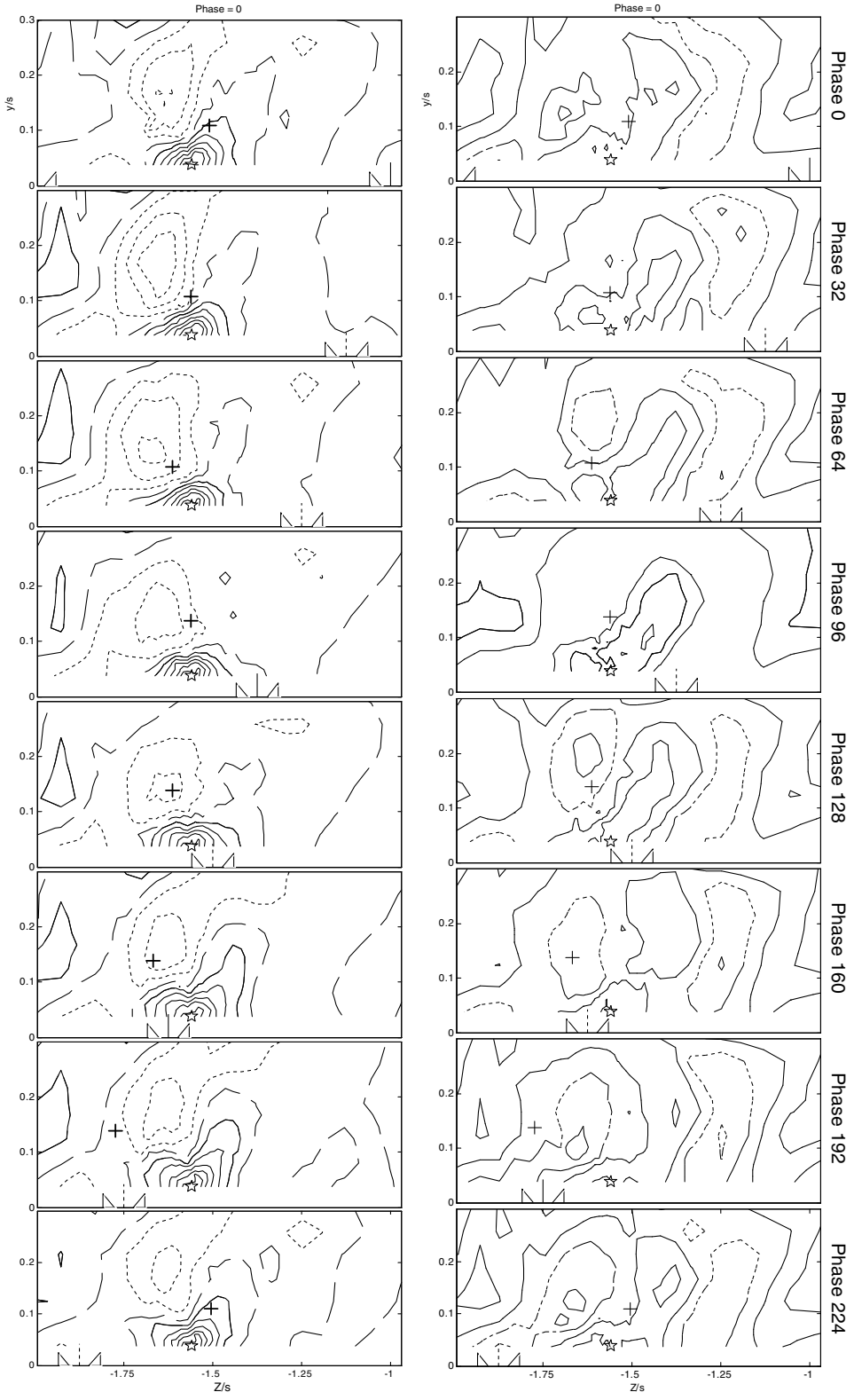

Fig. 4 Contours for 3.3%c tip gap at $X/s = 0.944$: a) of phase-averaged two-point correlation coefficient $\langle R_{uu} \rangle$, and b) of $R_{uu} - \langle R_{uu} \rangle$. Contours are in steps of 0.1 from −1 to 1, dotted-negative levels, dashed-zero, solid-positive levels. The triangle pairs indicate the pitchwise location of the vortex generators, which is given in Table 2. The pentagram denotes the fixed-probe position and the plus sign denotes the phase-averaged vortex center.

vortex region and is lower than that of R_{uu} apart from the vortex region, because the periodic fluctuations are not included. When the vortex generators move across the passage, the shape and location of the most negative correlation region changes and wanders with phase, and the location of correlation peak, of course, does not change. The other part of the negative correlation arc outside the vortex region has a very low magnitude and fluctuates a lot with the phase. For R_{uu}-$\langle R_{uu}\rangle$, no obvious large vortical structure is seen within the vortex region; the magnitude is much less than $\langle R_{uu}\rangle$ there, but it is higher than $\langle R_{uu}\rangle$ outside the vortex region. The scale of it is obviously larger than that of $\langle R_{uu}\rangle$. Other phase-averaged two-point correlations also have the same features shown in the corresponding time-averaged correlations and have a high magnitude within the vortex region.

The different flow patterns suggest that periodic motions are in large scale, that they exist within and outside the vortex region, and that they appear to be the variation and wandering seen in the tip-leakage-vortex shape and structure, which is consistent with the finding of MD [1]. The aperiodic motions are strong, especially within the tip-leakage-vortex region, though the vortex itself periodically varies a lot with phase.

Wenger et al. [6] took time-averaged two-point correlation measurements in the same facility at tip gap $1.65\%c$, but without the moving wall and generators. The measurement-plane location is $X/s = 1.664$ and the fixed-probe location ($y_f/s = 0.041$, $Z_f/s = -2.54$) also lies underneath the center of the tip-leakage vortex. The data are plotted in Fig. 5 in the same format as Fig. 3, except that it is plotted with respect to Δy and ΔZ, the distance between the moving and fixed probes. The two sets of correlation data look very similar, though there is much difference in the test conditions. The comparison between Figs. 3 and 5 shows that almost all of the components have similar shapes except R_{vu} and R_{vw}. This suggests that the tip-leakage vortex has a similar structure in both flows, independent of the tip-gap size, inflow disturbance, and wall motion. This also implies that the inflow disturbances do not change the basic turbulence structure, they only regulate them in some way. Comparing the R_{uu} component of the two sets of data, we can see that one major difference is that the magnitude and coverage region of current correlation functions are larger than those of the Wenger et al. data. For the Wenger et al. data, the correlation is zero outside the tip-leakage-vortex region, but the current time-averaged correlation almost extends across the whole measurement section. This may because of the larger tip-leakage vortex due to the larger tip gap of $3.3\%c$ and the unsteady motion of the tip-leakage vortex due to the vortex generators. The current phase-averaged correlation looks more like the Wenger et al. data, because the correlation level is lower away from the fixed point, though it periodically varies with phase. This implies that aperiodic motions are likely associated with the undisturbed tip-leakage vortex, and the inflow disturbances create the periodic larger-scale unsteadiness of the tip-leakage vortex. This also confirms the hypothesis of MD [1]: the unsteadiness of tip-leakage vortex is created by the inflow disturbances through interfering with the shedding of vorticity from the blade tips.

Table 2 Pitchwise location of the vortex generators

Phase	Z/s generator	
0	0.000	−1.000
32	−0.125	−1.125
64	−0.250	−1.250
96	−0.375	−1.375
128	−0.500	−1.500
160	−0.625	−1.625
192	−0.750	−1.750
224	−0.875	−1.875

Stochastic Estimation of Instantaneous Velocity Field

The two-point correlation coefficients are informative but provide information only in an implicit form, such that their physical flow cannot be fully appreciated by directly plotting them. To reveal the physical information encapsulated in these functions in a more explicit form, the method of stochastic estimation (Adrian [3]) is applied to the data. Adrian showed that the random velocity of the field, given the event data, can be estimated by conditional averaging, which can be approximated by linear stochastic estimate or identical linear mean square estimate. The latter provides a link between conditional averages and two-point correlations.

If we are given event data such as the instantaneous velocity fluctuation $u'_j(\vec{r}_f, \tau_p)$ over the phase-averaged velocity at the fixed point $\vec{r}_f$, the linear estimate of the velocity fluctuation of the field can be written as

$$u'_i(\vec{r}, \tau_p)|_e = A_{ij} u'_j(\vec{r}_f, \tau_p)$$

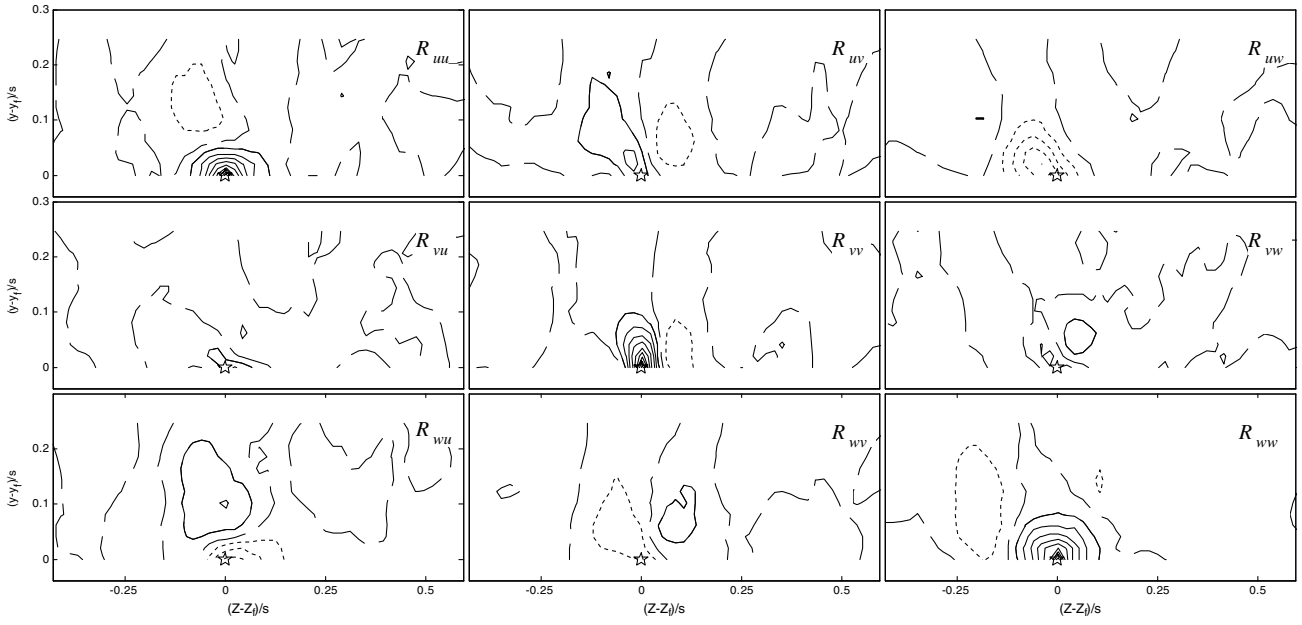

Fig. 5 The Wenger et al. [6] time-averaged zero-time-delay two-point correlation coefficients, plotted as a function of the relative position between the moving probe and the fixed probe at ($y_f/s = 0.041$, $Z_f/s = -2.54$); tip gap $1.65\%c$; stationary wall; and measurement-plane location $X/s = 1.664$.

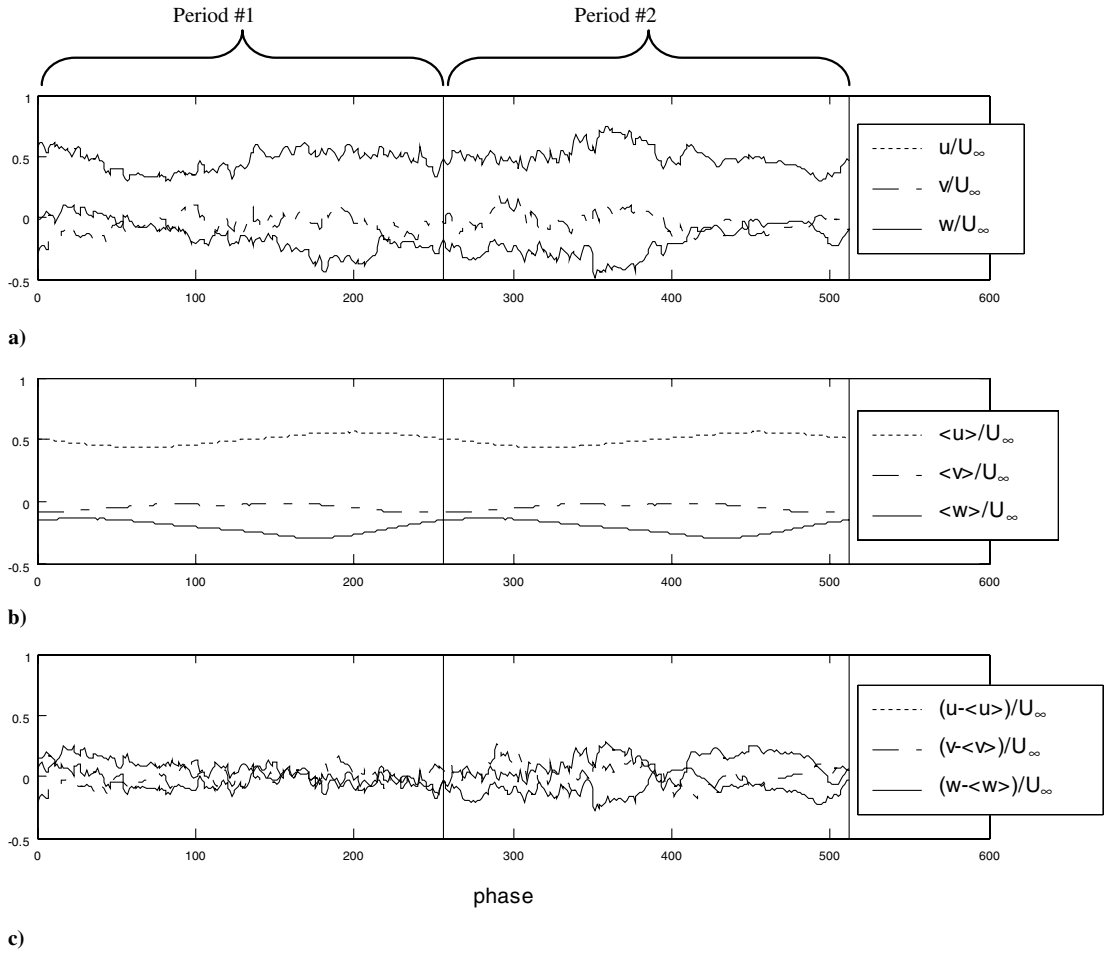

Fig. 6 Fixed-probe measurements at ($y_f/s = 0.038, Z_f/s = -1.56$) in two arbitrary successive periods for a) instantaneous velocities, b) phase-averaged velocities, and c) fluctuations.

Summation is implied and the coefficients $A_{ij}(\vec{r})$, functions of $\vec{r}$, and phase τ_p can be solved by the linear equations

$$A_{ij}\langle u_j'(\vec{r}_f)u_k'(\vec{r}_f)\rangle|_p = \langle u_i'(\vec{r})u_k'(\vec{r}_f)\rangle|_p$$

The estimated fluctuation is, of course, made up of the aperiodic fluctuations due to the generators and the real turbulence, which are smoothed out in the single-point phase-averaged mean data. The estimated instantaneous velocity field at each phase can thus be obtained by adding the estimated fluctuation field back to the phase-averaged velocity field.

To compute the estimated instantaneous velocity field, time-series data of two successive periods are arbitrarily extracted from the fixed-probe data. The instantaneous velocity, phase-averaged velocity, and instantaneous velocity fluctuations are plotted in Fig. 6. This plot clearly shows that the instantaneous fluctuations are in high frequency and their magnitude is so large that the phase-averaged flow features are completely submerged by the fluctuations.

Before the estimated velocity field results are presented, it should be mentioned that the estimated field always represents the conditional average of many realizations based on the given event data (Adrian [3]). If each realization is very similar to every other, the conditional average will look like the realization. If there is significant variation among realizations, then the conditional average only represents the mean effect of all realizations. This can also be expressed as follows: If the two-point correlation is significant, the estimation will be accurate; if the correlation is weak, then the estimation will just be a mean structure of the various realizations.

The estimated instantaneous velocity-fluctuation field is presented in Fig. 7, which shows the contours of streamwise velocity fluctuation, and Fig. 8, which shows the cross-velocity-fluctuation vectors. These plots display significant velocity fluctuations that are obviously aperiodic because the fluctuation field of each period is different even at same phase. Because the coefficient matrix $A_{ij}(\vec{r}, \tau_p)$ is a periodic function, the estimated aperiodic fluctuation is only due to the random fluctuation in all three directions at the fixed point. It can be seen that the aperiodic fluctuation is intense in the tip-leakage-vortex region in which the phase-averaged two-point correlations are larger. This is consistent with the aforementioned feature of aperiodic motions. The streamwise velocity-fluctuation contours reveal that at different phase times, organized positive (rush) and negative (retard) fluctuation regions with different shapes and structures coexist in the tip-leakage-vortex region. The maximum streamwise velocity fluctuation is about $\pm 0.15U_\infty$. The crossflow-velocity-fluctuation vectors reveal that at each phase time, clockwise/anticlockwise rotating vortical or doubletlike structures with different strength and center positions exist in the tip-leakage-vortex region. The maximum (v, w) velocity fluctuation is also about $\pm 0.15U_\infty$. The scale of these aperiodic turbulence structures is almost the same as the size of the tip-leakage vortex. Here, only the instantaneous fluctuation at eight equal-interval phase times are presented, but the data of all 256 phase times show that the fluctuation field varies significantly, even between two successive phases.

The complete estimated instantaneous velocity can be obtained by adding the estimated velocity fluctuations back to the phase-averaged velocity. Figures 9 and 10 show, respectively, the estimated instantaneous streamwise velocity and crossflow-vector field. It can be seen that the aperiodic fluctuations make significant changes to the phase-averaged velocity field. Each period, the velocity field appears to be different from the previous period.

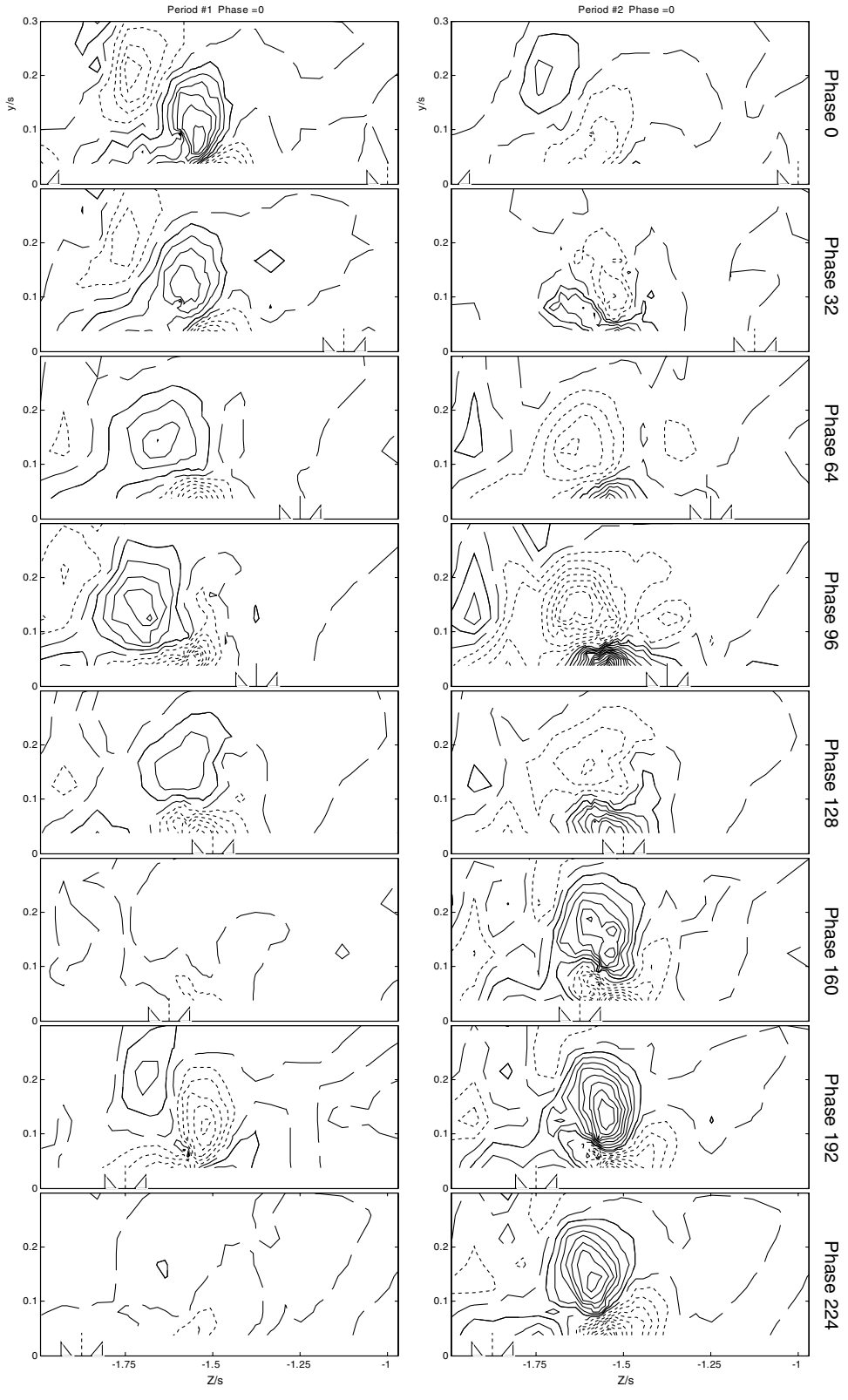

Fig. 7 Estimated instantaneous streamwise velocity fluctuation $(u - \langle u \rangle)/U_\infty$ of two successive periods obtained by using linear mean square estimation: a) period 1 and b) period 2. Contours are in steps of 0.01 from −0.2 to 0.2, dotted-negative levels, dashed-zero, solid-positive levels. The triangle pairs indicate the pitchwise location of the vortex generators, which is given in Table 2.

Wenger et al. [6] also visualized the time-averaged two-point space–time correlation in terms of linear stochastic estimation of the instantaneous velocity field associated with only the streamwise unit velocity fluctuation at the fixed point. The three-dimensional estimated flowfield determined using linear stochastic estimation and Taylor's hypothesis shows an intense elongated vortical structure skewed at an angle of about 30 deg to the vortex axis. This is consistent with the tip-leakage-vortex center path described by MD [1]. It also suggests that there is similar coherent structure existing inside the tip-leakage vortex even without the inflow disturbances.

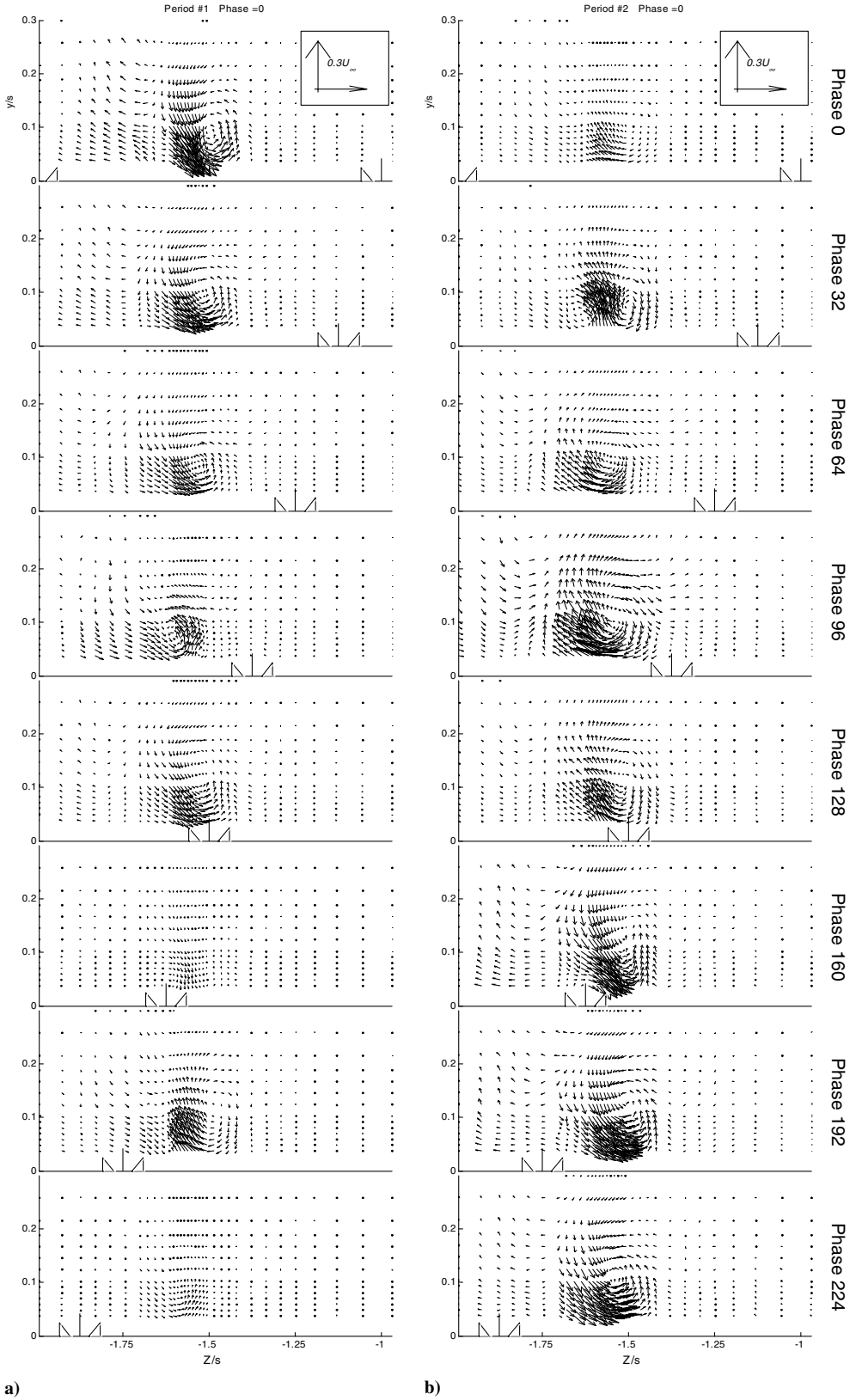

Fig. 8 Estimated instantaneous cross-velocity fluctuation $(v\text{-}\langle v\rangle, w-\langle w\rangle)/U_\infty$ of two successive periods obtained by using linear mean square estimation: a) period 1 and b) period 2. The triangle pairs indicate the pitchwise location of the vortex generators, which is given in Table 2.

Because there is a significant difference between the phase-averaged velocity field and the estimated instantaneous velocity field, it is interesting to look at the vorticity of the estimated instantaneous velocity field. Figure 11a shows the streamwise vorticity calculated based on the estimated instantaneous velocity of the first period. The contours are completely different from the vorticity calculated from the phase-averaged velocity field (shown in Fig. 12). Compared with the latter, the magnitude level of the maximum streamwise vorticity increased about five times. The high-vorticity region is located in the tip-leakage-vortex region, instead of underneath the blade like the vorticity of the phase-averaged data. There is also intense fluctuation with respect to both time and space in

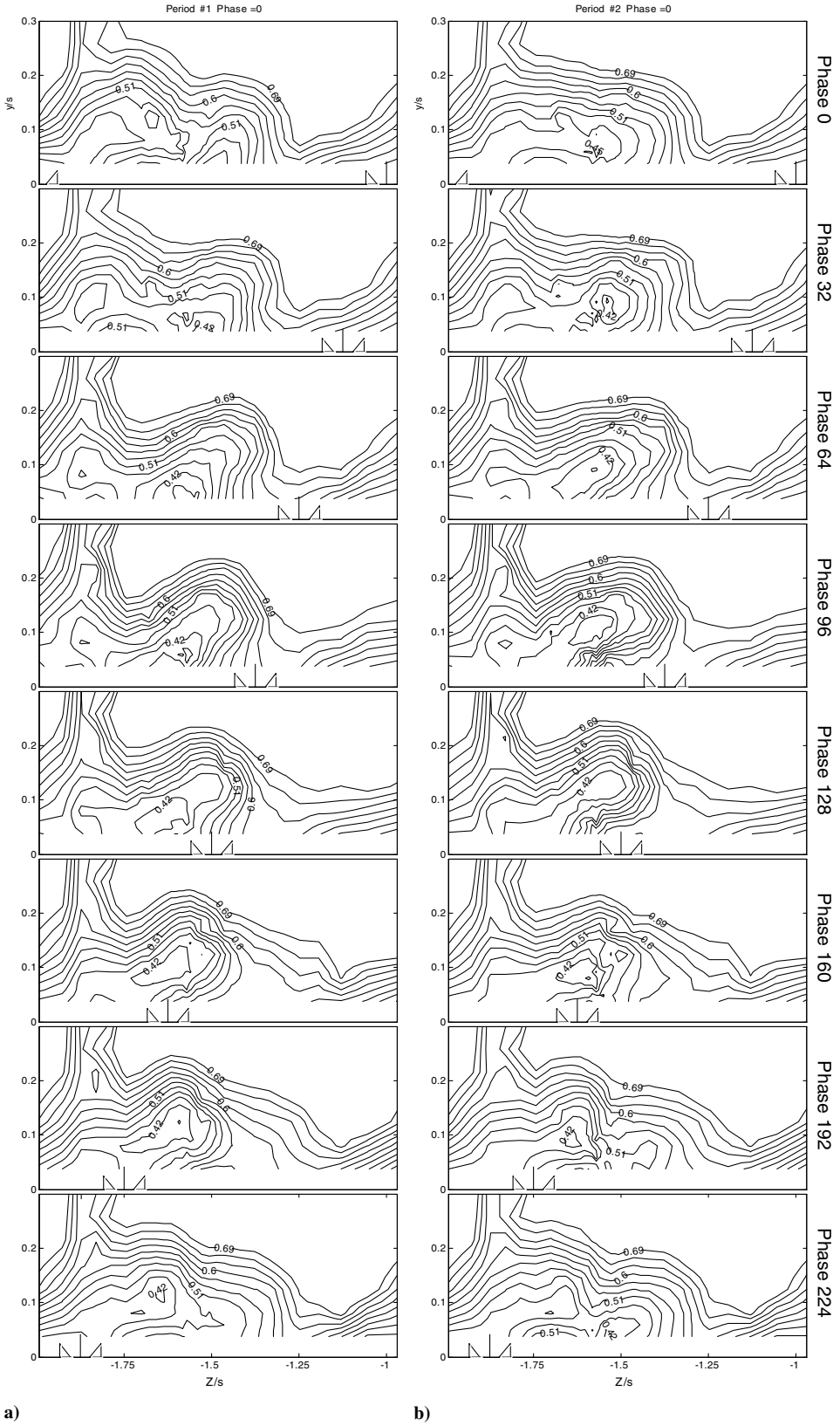

Fig. 9 Estimated instantaneous streamwise velocity u/U_∞ of two successive periods obtained by using linear mean square estimation: a) period 1 and b) period 2. Contours are in steps of 0.03 from 0.3 to 0.7. The triangle pairs indicate the pitchwise location of the vortex generators, which is given in Table 2.

the tip-leakage-vortex region. These differences are due to the estimated instantaneous fluctuations and the dense two-point measurement grid within the tip-leakage-vortex region.

It may be asked whether the vorticity calculated from the estimated instantaneous velocity field really presents the vorticity of the real flow. By looking at calculated vorticity data of all 256 phase times, it can be found that variation intensity with respect to time is so large that the whole field completely changes within one phase of bin time. This does not seem to be the real situation, because the timescale of the flow should on the same order as the length scale. By considering

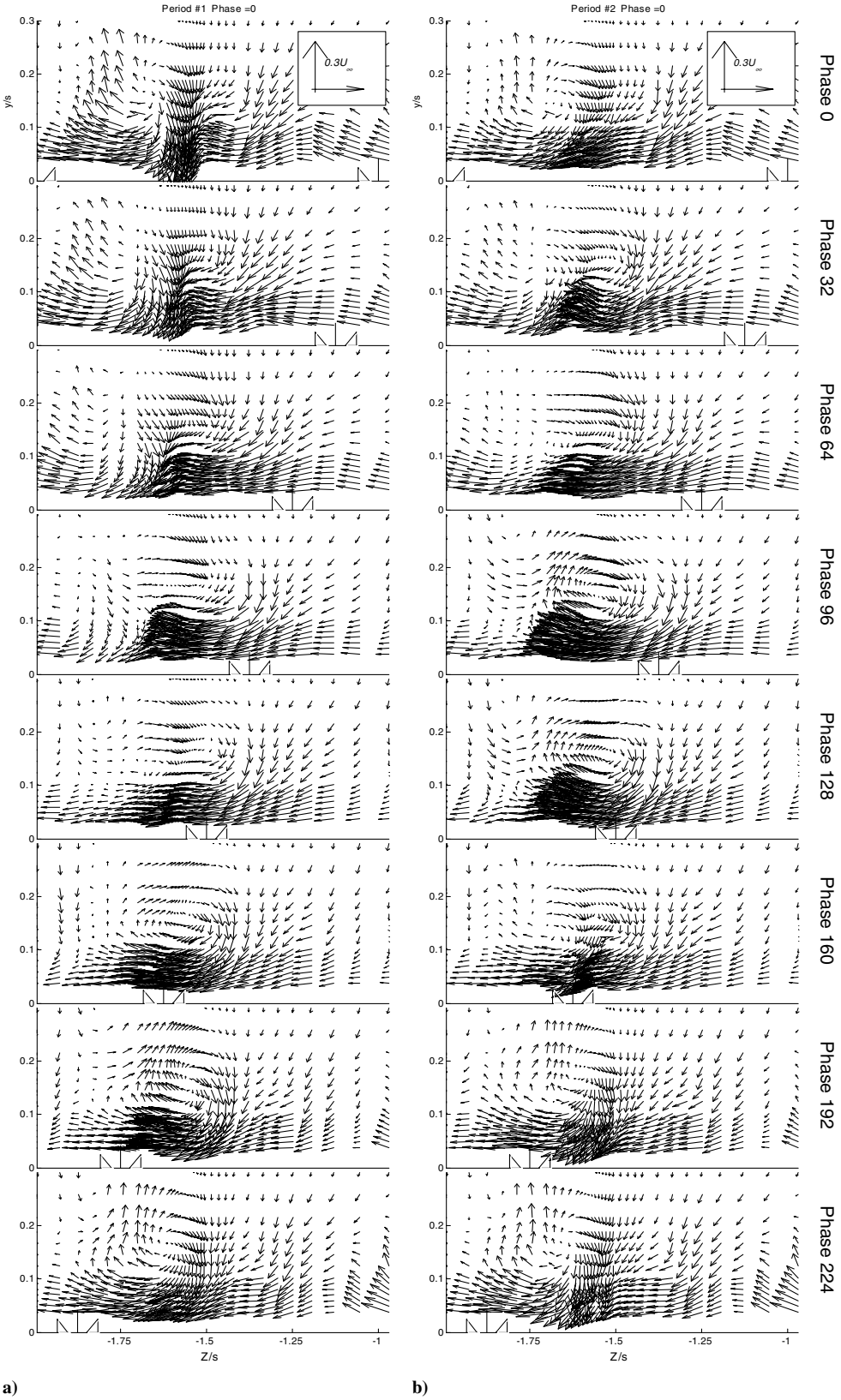

Fig. 10 Estimated instantaneous cross-velocity vectors $(v, w)/U_\infty$ of two successive periods obtained by using linear mean square estimation: a) period 1 and b) period 2. The triangle pairs indicate the pitchwise location of the vortex generators, which is given in Table 2.

the linear estimation equation, it is found that the fluctuation $u_j'(\vec{r}_f, \tau_p)$ at the fixed point in Fig. 6 may contain both low- and high-frequency components, but the coefficient matrix $A_{ij}(\vec{r}, \tau_p)$ is only the second-order two-point correlations and only contains the low-frequency components. So this linear equation may magnify the high-frequency fluctuations at the fixed point. To solve this problem and improve the prediction, a higher-order nonlinear estimation method is needed, which requires higher-order two-point correlations. Another simple way is to either remove the high-frequency-component fluctuation at the fixed point before applying the linear estimation or to smooth the results of the linear estimation along the time axis; here, the latter approach is used. A nine-point

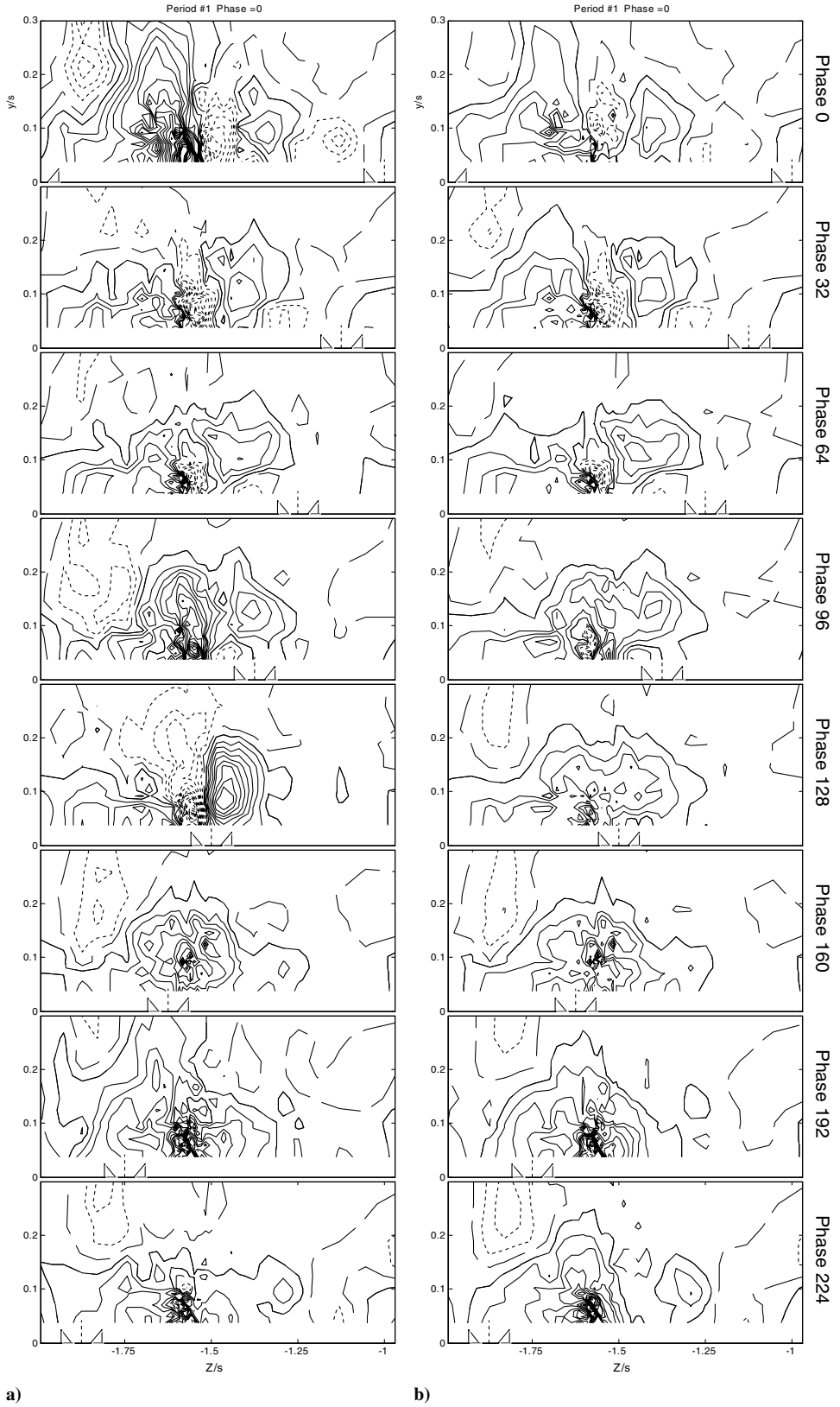

Fig. 11 Comparison of the streamwise vorticity $\Omega_x s/U_\infty$ of the estimated instantaneous velocity field (period 1): a) unsmoothed and b) smoothed. Contours in steps of 0.75 from −15 to 15, dotted-negative levels, dashed-zero, solid-positive levels. The triangle pairs indicate the pitchwise location of the vortex generators, which is given in Table 2.

averaging code is used to smooth the vorticity by averaging the vorticity date at each phase time over nine contiguous phases. The cutoff frequency implied by the nine-point average is 2.7 kHz, which implies a timescale that corresponds to an 8.3-mm (0.035-s) movement of the endwall relative to the blades or a 9.1-mm (0.039-s) movement of the freestream. These are still quite small compared with the large-scale fluctuations in structure of the tip-leakage flow, and so the averaging gives more reliable low-frequency unsteady behavior information at the cost of lower resolution in phase. After applying the averaging, the estimated velocity field is almost the same as the unsmoothed velocity field; however, the vorticity of the smoothed instantaneous velocity field, shown in Fig. 11b, looks

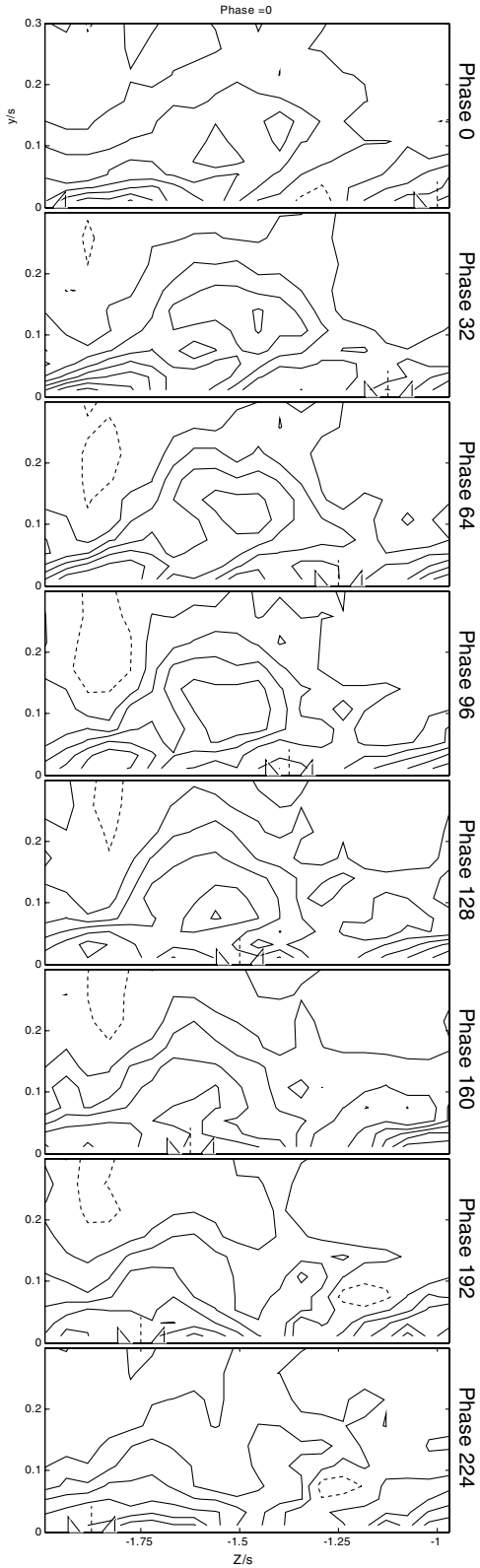

Fig. 12 Streamwise vorticity of phase-averaged velocity field. Contours in steps of 0.75 from −15 to 15, dotted-negative levels, dashed-zero, solid-positive levels. The triangle pairs indicate the pitchwise location of the vortex generators, which is given in Table 2.

more reasonable than the unsmoothed vorticity, though it is still unlike the vorticity of the phase-averaged data.

Conclusions

Phase-averaged two-point correlations are measured in the tip-leakage flow downstream of a simulated compressor rotor. The tip-leakage vortex is subject to the relative motion of the endwall and to the periodic disturbances of inflow vortices shed by the vortex-generator pairs attached and moving with the endwall. There are significant phase-averaged periodic fluctuations existing in the tip-leakage-vortex size, strength, position, and structure. The contribution of aperiodic fluctuations is greatly dominant in the total turbulence kinetic energy.

The measured time-averaged zero-time-delay two-point correlations reveal the presence of significant large-scale structures within the leakage vortex flow. The large periodic variation of the phase-averaged correlations away from the fixed point suggests that the large-scale periodic motions exist in the tip-leakage flow, which is consistent with the results of MD [1]. However, the organized pattern and large magnitude and scale of the phase-averaged two-point correlations at each phase time suggest that in addition to the periodic motions, organized, intense, large-scale aperiodic motion exists at each phase time within the tip-leakage-vortex region. These phase-averaged two-point correlations have patterns similar to that of the no-inflow-disturbances case. This implies that the inflow disturbances do not fundamentally change the mechanism of the tip-leakage vortex and confirms the hypothesis of MD [1]: they create large unsteadiness in tip-leakage vortex by influencing the shedding of vorticity from the blade tips.

Linear stochastic estimation is used to educe the instantaneous velocity field associated with the instantaneous velocity fluctuation at the fixed point in terms of the measured phase-averaged two-point correlations. The estimated instantaneous velocity fields show that significant aperiodic fluctuations exist in the tip-leakage-vortex region. The aperiodic fluctuations have a magnitude of less than $\pm 0.15 U_\infty$ in all three velocity directions and appear to be organized large-scale structures. The streamwise fluctuations appear to be coexisting "rush" and "retard" regions with different shape, and the crossflow fluctuations appear to be clockwise/anticlockwise or doubletlike rotating vortical structures with different strength and center positions. These aperiodic fluctuations make the estimated instantaneous velocity field significantly different from the phase-averaged periodic velocity field. The vorticity calculated based on the estimated instantaneous velocity fields is consequentially different from that of the phase-averaged velocity field. The magnitude level of the former is significant larger than that of the latter. Intense vorticity fluctuations with respect to both time and space exist in the tip-leakage-vortex region.

Acknowledgements

The authors would like to thank the Office of Naval Research, in particular, Ki-Han Kim, for the support of this work through grant N00014-99-1-0294. The assistance of Chittiappa Muthanna with performing measurements is gratefully acknowledged. Numerical results from the experiments described here are available from the authors' Web site, http://www.aoe.vt.edu/flowdata.

References

[1] Ma, R., and Devenport, W. J., "Unsteady Periodic Behavior of a Disturbed Tip Leakage Flow," *AIAA Journal*, Vol. 44, No. 5, 2006, pp. 1073–1086.

[2] Ma, R., and Devenport, W. J., "Tip Gap Effects on the Unsteady Behavior of a Tip Leakage Vortex," *AIAA Journal*, Vol. 45, No. 7, 2007, pp. 1713–1724.

[3] Adrian, R. J., "Stochastic Estimation of the Structure of Turbulent Fields," *Eddy Structure Identification*, edited by J. P. Bonnet, Springer, New York, 1996, pp. 145–195.

[4] Devenport, W. J., Muthanna, C., Ma, R., and Glegg, S. A. L., "Two-Point Description of Wake Turbulence with Application to Noise Prediction," *AIAA Journal*, Vol. 39, No. 12, 2001, pp. 2302–2307.

[5] Devenport, W. J., and Glegg, S. A. L., "Modeling the Two-Point Space–Time Correlation of Turbulence in a Fan-Wake Type Flow," 7th AIAA/CEAS Aeroacoustics Conference, Maastricht, The Netherlands, AIAA Paper 2001-2241, 28–30 May 2001.

[6] Wenger, C. W., Devenport, W. J., Wittmer, K. S., and Muthanna, C., "The Wake of a Compressor Cascade with Tip Gap, Part 3: Two-Point Statistics," *AIAA Journal*, Vol. 42, No. 11, 2004, pp. 2341–2346.

[7] Ma, R., "Unsteady Turbulence Interaction in a Tip Leakage Flow Downstream of a Simulated Axial Compressor Rotor," Ph.D. Dissertation, 2003, Virginia Polytechnic Inst. and State Univ., Blacksburg, VA; also http://scholar.lib.vt.edu/theses/available/etd-06172003-122153/.
[8] Muthanna, C., and Devenport, W. J., "The Wake of a Compressor Cascade with Tip Gap, Part 1: Mean Flow and Turbulence Structure," *AIAA Journal*, Vol. 42, No. 11, 2004, pp. 2320–2331.
[9] Kline, S. J., and McClintock, F. A., "Describing Uncertainties in Single Sample Experiments," *Mechanical Engineering*, Vol. 75, No. 1, 1953, p. 38.

K. Ghia
Associate Editor